Study of applied magnetic field magnetoplasmadynamic thrusters with particle-in-cell and Monte Carlo collision. II. Investigation of acceleration mechanisms

Cite as: Phys. Plasmas **19**, 073108 (2012); https://doi.org/10.1063/1.4737104
Submitted: 09 March 2012 . Accepted: 20 June 2012 . Published Online: 13 July 2012

Hai-Bin Tang, Jiao Cheng, Chang Liu, and Thomas M. York

Study of applied magnetic field magnetoplasmadynamic thrusters with particle-in-cell and Monte Carlo collision. II. Investigation of acceleration mechanisms

Hai-Bin Tang,[1] Jiao Cheng,[1] Chang Liu,[1] and Thomas M. York[2]
[1]*School of Astronautics, Beijing University of Aeronautics and Astronautics, Beijing 100191, China*
[2]*Aeronautical and Astronautical Engineering Department, Ohio State University, Columbus, Ohio 43235, USA*

(Received 9 March 2012; accepted 20 June 2012; published online 13 July 2012)

The particle-in-cell method previously described in paper (I) has been applied to the investigation of acceleration mechanisms in applied-field magnetoplasmadynamic thrusters. This new approach is an alternative to magnetohydrodynamics models and allows nonlocal dynamic effects of particles and improved transport properties. It was used to model a 100 kW, steady-state, applied-field, argon magnetoplasmadynamic thruster to study the physical acceleration processes with discharge currents of 1000–1500 A, mass flow rates of 0.025–0.1 g/s and applied magnetic field strengths of 0.034–0.102 T. The total thrust calculations were used to verify the theoretical approach by comparison with experimental data. Investigations of the acceleration model offer an underlying understanding of applied-field magnetoplasmadynamic thrusters, including the following conclusions: (1) swirl acceleration mechanism is the dominant contributor to the plasma acceleration, and self-magnetic, Hall, gas-dynamic, and swirl acceleration mechanisms are in an approximate ratio of 1:10:10:100; (2) the Hall acceleration produced mainly by electron swirl is insensitive to the change of externally applied magnetic field and shows only slight increases when the current is raised; (3) self-magnetic acceleration is normally negligible for all cases, while the gas-dynamic acceleration contribution increases with increasing applied magnetic field strength, discharge current, and mass flow rate. © *2012 American Institute of Physics*. [http://dx.doi.org/10.1063/1.4737104]

NOMENCLATURE

$\boldsymbol{A}$ = magnetic vector potential
$\boldsymbol{B}$ = magnetic field, T
$\boldsymbol{E}$ = electric field, V/m
E_i = first ionization energy, J
e = elementary charge, C
I = discharge current, A
$\boldsymbol{j}$ = current density, A/m^2
k = Boltzmann constant
M_i = ion mass, kg
m = particle mass, kg
$\dot{m}$ = mass flow rate, kg/s
n = number density,/m^3
r = electrode radial, m
T = thrust, N
t = time, s
$\boldsymbol{U}$ = velocity, m/s
$\boldsymbol{X}$ = location vector, m
φ = plasma potential, V
ε_0 = free-space permittivity
μ_0 = permeability of free space, H/m
λ_D = Debye length, m

Subscripts

a = anode
ap = applied-field
c = cathode
e = electron
gd = gas-dynamic
i = ion
j = node
sf = self-field
z, r, θ = physical dimensions: axial, radial, azimuthal

I. INTRODUCTION

Magnetoplasmadynamic (MPD) thrusters are electromagnetic accelerators in which the plasma is accelerated to high velocities through Lorentz body force from the interaction of currents and magnetic fields (both self-generated and applied). Consequently, they are also referred to as Lorentz force accelerators. Comprehension of the underlying acceleration mechanisms is a necessary basis for MPD design that can lead to improved thruster performance. Self-field MPD thrusters have a relatively well understood acceleration mechanism, as was discussed by Choueiri.[1] However, there is no clear understanding of the detailed physics inherent in applied field MPD thrusters.[2]

A combined experimental and theoretical approach has been used to address the question of acceleration processes in applied field MPD thrusters over the last 40 years. Experimental research has produced results from a limited number of thrusters. Using these experimental data, theoretical studies have produced several models that capture the general trends and magnitudes of experimental devices. All previous

efforts have concentrated on either modeling the acceleration processes or identifying evidence of mechanism inferred from some assumptions and experiments.[3]

One exceptional earlier experimental study of an applied-field MPD thruster was that of Fradkin[4,5] with a 10–35 kW lithium thruster. He observed that thrust seemed to vary linearly with the product of discharge current and applied magnetic field strength, allowing a simple empirical expression for thrust that formula could be recovered with the assumption that the rotational energy was completely converted to axial kinetic energy.

In an experimental study with a 100 kW steady-state applied-field MPD thruster, Mayers[6,7] investigated a range of operating conditions for applied magnetic field strengths of 0.03–0.2 T, discharge currents of 750–2000 A, and argon and hydrogen propellant at mass flow rates of 25–140 mg/s. The results showed that thrust increased linearly with increasing applied magnetic field strength and discharge current, while it increased parabolically with increasing anode radius and decreased with increasing cathode radius. Thrust magnitudes increased with increasing electrode length, but had no correlation with geometry, mass flow rate, and propellant type.

In the theoretical study of acceleration mechanisms in applied-field MPD thrusters, Krulle[8] established a model based on flow equations and the assumption that plasma was fully ionized. The model neglected the induced self-field and considered operation at low current density and mass flow rate. It was found that the plasma pressure forces balancing the radial magnetic confinement held a substantial part of the total thrust.

Tanaka and Kimura[9] utilized a set of electromagnetic and fluid equations to model the applied field MPD thruster at operation with argon at 0.1 g/s, discharge current of 1000–2000 A, and applied magnetic field strength of 0.1–0.2 T. The results demonstrated that the plasma rotation was produced and converted into axial kinetic energy through expansion in a magnetic nozzle.

Based on the hypothesis that all the electromagnetic forces are converted into axial-directed kinetic energy, Sasoh and Arakawa[10,11] considered Hall, swirl, and self-magnetic acceleration mechanisms in an applied-field MPD thruster. The developed thrust formula indicated that Hall and swirl accelerations are the dominant modes at low discharge current ($I < 400$ A) and mass flow rate ($\dot{m} < 30$ mg/s). The predicted thrust was lower than the experimental values for higher discharge current and mass flow rate.

Mikellides, Turchi, and Roderick[3,12] used the magnetohydrodynamic code MACH2 to model a 100 kW, steady-state, applied-field, argon MPD thruster. This was a time-dependent, two-dimensional, multi-temperature MHD code that requires the input of exact transport coefficients in the plasma flows. The numerical modeling was performed for applied magnetic field strengths of 0.034–0.102 T and discharge currents of 750–1250 A. The computation results offered the new standpoint that viscous heating and conversion of thermal energy to axial directed kinetic energy was the main acceleration mechanism. A simple thrust expression was developed with the new insights. However, understanding of processes for transformation of rotational energy to directed axial motion, as well as related losses, remains inferential and new analyses are needed to identify the active mechanisms.

Along with the theoretical research and calculation of applied-field MPD thrusters are trend to a multidimensional and complicated systematic process, Fruchtman *et al.*[13] provided a new idea of the theoretical study. A simple, quasi one-dimensional model was established to calculate the momentum delivered to the plasma in a magnetic nozzle with a good accuracy. The model can be used in experiments for a quick and simple estimate of the thrust by the measured axial magnetic field on axis.

Investigation of acceleration mechanisms is the foundation for optimum thruster design and other physical problems, such as the operation physical process. Previous theoretical efforts attempted to address the macroscopic characteristics of acceleration processes in an applied-field MPD thruster. Based on various experiments, several models have been proposed using physical assumptions. The models investigated thrust generation in order to understand the acceleration mechanisms and so determine the dominant thrust components. The goal of the previous works was to further resolve the exact nature of the actual acceleration mechanisms that capture all the experimental data and develop the physical comprehension of the model. The formulation of accurate expressions for thrust as a function of the operation parameters (discharge current, applied-field strength, and mass flow rate) has as not yet been completed. Accordingly, a general formula for thrust in accordance with all relevant experimental data and an identification of the most efficient acceleration mode is still the subject of consideration.

Actual acceleration mechanisms in the applied-field MPD thruster are complicated, so a simple underlying theoretical approach is required rather than beginning with model assumptions for understanding of the experimental results. In paper (I), the particle-in-cell with Monte Carlo collision (PIC-MCC) computation methods were described in detail, and the results were verified by comparison with experiment. In this paper (II), the new approach uses the PIC-MCC method to define the acceleration mechanisms in a 100 kW applied-field MPD thruster. The study focuses on the identification of the dominant acceleration mechanisms. This method concentrated on obtaining the acceleration mode in terms of microcosmic aspects, rather than considering the correlation between thruster performance and operation parameters. The objective of this work is to identify electromagnetic and gas-dynamic accelerations and provides understanding of the main acceleration mechanism based on particle dynamics.

In Sec. II, previous acceleration models are reviewed and summarized. In Sec. III, the numerical model of the acceleration mechanisms with PIC-MCC method is described, and in Sec. IV, this new approach is applied to investigate the underlying acceleration processes, and there is a discussion of the simulation results.

II. PREVIOUS MODELS FOR THRUST EVALUATION

In general, the MPD thruster consists of a central cathode surrounded by a concentric anode. Between the anode

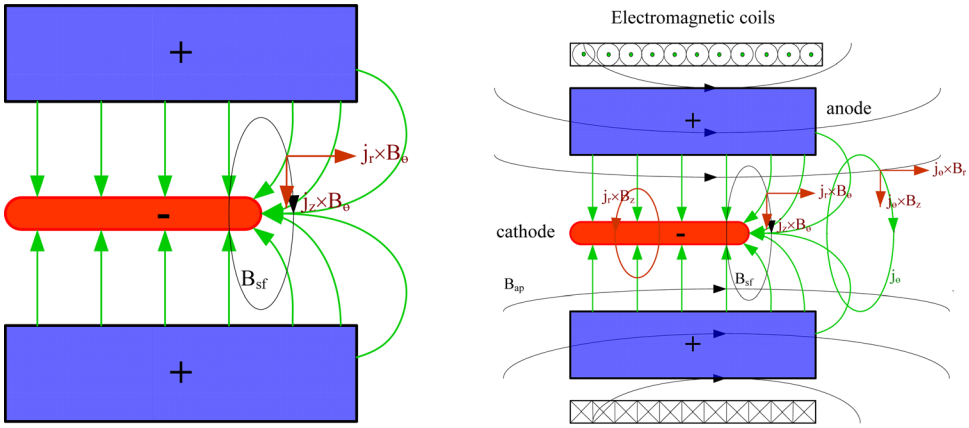

(a) Self-field MPD thruster

(b) Applied-field MPD thruster

FIG. 1. MPD thruster schematic with applied and induced fields and currents and electromagnetic forces shown.

and cathode, a high-current arc exists which ionizes and accelerates a gas propellant. MPD thrusters are envisioned as using the Lorentz force from interacting currents and magnetic fields to accelerate the plasma to high speeds as shown in Fig. 1. In a self-field MPD thruster, an axial thrust was produced by the interaction of a self-induced, azimuthal magnetic field B_θ arising from the current flow and radial component of the plasma current j_r. The applied-field MPD thruster shares coaxial electrodes with the addition of an external coil around the outside of the anode. The coil can produce applied axial and radial magnetic field components. These interact with the plasma currents to produce a variety of force components: azimuthal ($j_r \times B_z$, $j_z \times B_r$), radial ($j_\theta \times B_z$), and additional axial ($j_\theta \times B_r$).[14]

The acceleration processes inherent in the MPD thrusters can be separated into "self-field" acceleration and "applied-field" acceleration. The theories which have been considered for modeling, the self-field and applied-field acceleration components and to predict thrust have been given in the previous studies.[15] The fundamental assumptions and relationships will be reviewed here to clarify those model descriptions.

In the self-field thruster, the acceleration is dependent purely upon the self-induced field. A relatively well understood thrust mechanism has been described. The purely electromagnetic thrust, T_{sf}, can be expressed with the Maecker formula[16]

$$T_{sf} = \frac{\mu_0 I^2}{4\pi}\left[\ln\left(\frac{r_a}{r_c}\right) + \frac{3}{4}\right], \tag{1}$$

Choueiri[1] has modified this theory by supposing two regimes of behavior, partially and fully ionized. The self-field thrust then takes the form

$$T_{sf} = \begin{cases} \dfrac{\dot{m} U_a I}{I_{fi}} & u_e < U_a \quad \textit{partially ionized} \\ \dfrac{\mu_0 I^2}{4\pi}\left[\ln\left(\dfrac{r_a}{r_c}\right) + \dfrac{3}{4}\right] & u_e > U_a \quad \textit{fully ionized} \end{cases}, \tag{2}$$

where U_a is the Alfvén critical ionization velocity and I_{fi} is the fully ionized plasma current as

$$U_a = \sqrt{\frac{2eE_i}{M_i}}, \quad I_{fi} = \sqrt{\frac{4\pi\dot{m}U_a}{\mu_0}\left[\ln\left(\frac{r_a}{r_c}\right) + \frac{3}{4}\right]^{-1}}. \tag{3}$$

Using simplifying assumptions (e.g., the magnetic field is azimuthal and uniform), Fruchtman[17] presented a one-dimensional theoretical model. The formula indicated that the thrust was related to the mass flow rate, electric potential, discharge current, magnetic field strength, and thruster diameter.

A number of theories have been proposed to explain the acceleration mechanisms in applied-field MPD thrusters. Based on experiments in specific current and applied field ranges, the observation was made that there was a linear variation of thrust with the product of discharge current and applied magnetic field strength. On the assumption that the azimuthal kinetic energy was all converted into axial kinetic energy, Fradkin[4] proposed a rotation model from which the applied-field thrust can be expressed as

$$T_{ap} = k(r, \dot{m}) I B_{ap}, \tag{4}$$

where $k(r, \dot{m})$ is the thrust coefficient. The model developed from numerical studies of Mikellides and Turchi[12] concluded that the plasma rotation includes a radial shear which heats the plasma and enhances the thermal thrust component. This acceleration mechanism gave a scaling of thrust with the product of current and applied magnetic field and included mass flow rate dependence.

$$T_{ap} = C(r)\sqrt{\dot{m} I B_{ap}}, \tag{5}$$

where $C(r)$ is the thrust constant, depends on the geometry and the propellant species. The acceleration model applicable to the widest range of operations appeared to be the combined fully ionized self-field and viscous heating applied-field model. The total thrust could then be written as

$$T_{total} = T_{sf} + T_{ap}. \quad (6)$$

Another alternative simplified applied-field MPD model was proposed by Tikhonov and Semenikhin.[18] The standard Tikhonov model described the thrust as a combination of three components including gas dynamic thrust T_{gd}, applied magnetic field thrust T_{ap}, and self induced magnetic thrust T_{sf}, as

$$T_{gd} = K_{gd} a_0 \dot{m}, \quad (7)$$

$$T_{ap} = 2K_{ap} I B_{ap} r_a, \quad (8)$$

$$T_{sf} = \frac{\mu_0 I^2}{4\pi}\left[\ln\left(\frac{r_a}{r_c}\right) + \frac{3}{4}\right], \quad (9)$$

where K_{gd} is the gas dynamic thrust coefficient, a_0 is the sonic velocity, and K_{ap} is the applied field thrust coefficient. Then, the total thrust can be expressed by

$$T_{total} = T_{gd} + T_{ap} + T_{sf}. \quad (10)$$

The above noted investigations do not provide conclusive evidence as to the acceleration processes occurring in applied-field MPD thrusters. The aforementioned models, furthermore, are not able to capture all the available experimental evidences. The discussions had focused on the applicability of some of the theories to some existing applied-field thruster data. In fact, the formulation of modals for the complete combined acceleration mechanisms involved in applied-field MPD thrusters may not be straightforward. A complete theory or approach based on underlying physical principles rather than model components and experiential relations is required.

III. ANALYTICAL MODELING

A. Acceleration model

The applied-field MPD thruster is a hybrid accelerator with electromagnetic and gas dynamic processes both contributing to the acceleration. The acceleration principle of the thruster is demonstrated in Fig. 1(b). Four major acceleration modes are considered to be effective;[19–21] briefly, the four modes are as follows:

(1) Self-magnetic acceleration: The radial current j_r interacts with the azimuthal magnetic field B_θ induced by the current flow, therefore producing an electromagnetic force $j_r \times B_\theta$ in the axially outward direction and $j_z \times B_\theta$ in the radially inward direction. The axial component contributes directly to thrust and the radial component adds to the thrust indirectly through increasing the radial particle velocity to increase the radial current.
(2) Swirl acceleration: The interactions of applied current (j_r, j_z) and applied magnetic field (B_z, B_r) produces azimuthal Lorentz force ($j_r \times B_z$, $j_z \times B_r$), which imparts rotational kinetic energy to the plasma. The assumption that the rotational kinetic energy can be converted into axial kinetic energy through expansion in a physical or magnetic nozzle processes was the basis for the previous theoretical efforts. However, such conversion mechanism is not well understood.
(3) Hall acceleration: The azimuthal current j_θ induced mainly by Hall effects interacts with the applied magnetic field (B_z, B_r), yielding electromagnetic force components ($j_\theta \times B_z$, $j_\theta \times B_r$) in a similar manner to the self-magnetic case. However, the direction of the force components (positive or negative contribution to thrust) is not clear in the general depiction. There is still debate about evidence for Hall acceleration in the applied-field MPD thrusters.
(4) Gas dynamic acceleration: This acceleration mode is similar to that in an electro-thermal arcjet. The working plasma is heating up by Joule heating and it then expands in a physical or magnetic nozzle. The additional gas dynamic thrust is associated with plasma pressure. Although this acceleration mechanism is not categorized as part of the electromagnetic acceleration, for practicality it needs to be taken into consideration.

In the applied-field MPD thruster, practicable thrust portions are due to the different acceleration mechanisms. The self-magnetic thrust is treated as T_{self}; thrust produced through the conversion of swirl motion is designated as T_{swirl}; thrust production depending on azimuthal currents is called T_{hall}. The remaining axial pressure component exerted on the nozzle is termed T_{gd}. Generally, with the assumption that rotational energy is converted completely to axial kinetic energy, total thrust can be described as

$$T_{total} = T_{self} + T_{swirl} + T_{hall} + T_{gd}. \quad (11)$$

Under the simplifying assumption that each thrust portion is generated by the conversion of attributed energy added to axial useful energy, another definition of total thrust is obtained as follows:[22]

$$T_{total} = [(T_{self} + T_{hall})/2] + \{[(T_{self} + T_{hall})/2]^2 + T^2{}_{swirl} + T^2{}_{gd}\}^{1/2}. \quad (12)$$

Using the above formula, the order of magnitude for each acceleration mechanism can be estimated. The quantitative

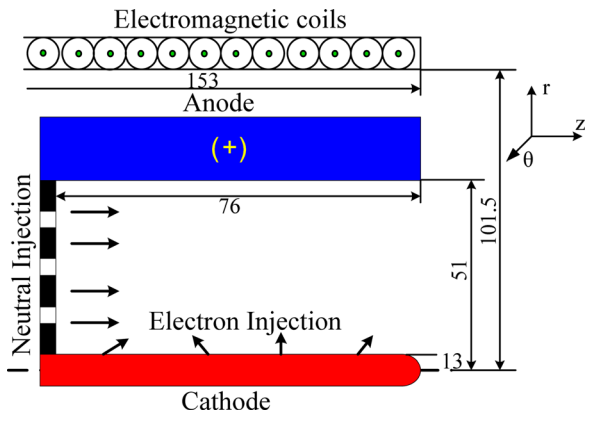

FIG. 2. Configuration of applied-field MPD thruster simulated.

calculation can be used to determine the dominant acceleration mechanism and then to quantitatively compute each acceleration effect. The new approach of the PIC method was used in this study to define magnitudes of each of the thrust components.

The discharge region is surrounded by an anode and cathode. An axisymmetric acceleration channel is assumed as is shown in Fig. 2. Considering cylindrical coordinates (z, r, θ), the current density $\boldsymbol{j}$, magnetic field $\boldsymbol{B}$, plasma velocity $\boldsymbol{u}$, and electric field $\boldsymbol{E}$ are assumed to have the following components, respectively:

$$\boldsymbol{j} = \begin{bmatrix} j_z \\ j_r \\ j_\theta \end{bmatrix}, \quad \boldsymbol{B} = \begin{bmatrix} B_z \\ B_r \\ B_\theta \end{bmatrix}, \quad \boldsymbol{u} = \begin{bmatrix} u_z \\ u_r \\ u_\theta \end{bmatrix}, \quad \boldsymbol{E} = \begin{bmatrix} E_z \\ E_r \\ 0 \end{bmatrix}. \tag{13}$$

As in a standard PIC model, the velocity and trajectory of each individual particle is integrated from Newton's second law.

$$\frac{dm\boldsymbol{u}}{dt} = q\,(\boldsymbol{E} + \boldsymbol{u} \times \boldsymbol{B}), \quad \frac{d\boldsymbol{X}}{dt} = \boldsymbol{u}. \tag{14}$$

It is assumed that only 1° of ionization may exist $(q = e)$. The integrations used a standard leapfrog scheme. The macroscopic fields were solved by Maxwell's equations.

$$\begin{aligned} \nabla^2\phi &= -\frac{e}{\varepsilon_0}(n_i - n_e), \\ \boldsymbol{E} &= -\nabla\phi, \\ \nabla \times \boldsymbol{B} &= \mu_0 \boldsymbol{j}, \\ \nabla \cdot \boldsymbol{B} &= 0. \end{aligned} \tag{15}$$

The applied magnetic field is static and consists of radial component and axial component. The azimuthal self-magnetic field (field induced by the discharge current) is considered, and radial and axial self-magnetic components are negligible compared to the applied field. The magnetic vector potential $(\boldsymbol{A})$ can be defined by

$$\boldsymbol{B} = \nabla \times \boldsymbol{A}. \tag{16}$$

The vector potential equation can be expressed as

$$\nabla^2 \boldsymbol{A} = -\mu_0 \boldsymbol{j}. \tag{17}$$

B_z and B_r include the intrinsic applied magnetic field and the induced magnetic field which are given by the derivatives of the magnetic vector potential as shown below.

$$\begin{aligned} B_z &= B_{ap,z} + \frac{1}{r}\frac{\partial r A_\theta}{\partial r} \approx B_{ap,z}, \quad B_r = B_{ap,r} - \frac{\partial A_\theta}{\partial z} \approx B_{ap,r}, \\ B_\theta &= \frac{1}{r}\frac{\partial A_r}{\partial z} - \frac{1}{r}\frac{\partial A_z}{\partial r}. \end{aligned} \tag{18}$$

At each time step, electrons are injected into the simulation region from the surface of cathode. Considering electron-neutral ionization collisions modeled by Monte Carlo technique, the singly charged ions and secondary electron are created at the primary electrons' locations at the end of each time step. The plasma current can be obtained by

$$\boldsymbol{j} = e(n_i \boldsymbol{u}_i - n_e \boldsymbol{u}_e). \tag{19}$$

The directed electromagnetic kinetic energy produced by axial forces contributes directly to thrust. A large fraction of the energy imparted by the forces in other directions can be converted to axial energy through the expansion in a magnetic nozzle. Under the assumption that the indirect energy can be converted completely into axial kinetic energy, then, quantifying the thrust portion produced by each mechanism, the following formula can be used:

$$T_{self} = \int_V \sqrt{(j_r B_\theta)^2 + (j_z B_\theta)^2}\, dV, \tag{20}$$

$$T_{swirl} = \int_V (-j_r B_z + j_z B_r)\, dV, \tag{21}$$

$$T_{hall} = \int_V \sqrt{(j_\theta B_r)^2 + (j_\theta B_z)^2}\, dV. \tag{22}$$

The gas dynamic thrust can be estimated from the equation

$$T_{gd} = \int_S (k n_i T_i + k n_e T_e + k n_a T_a)\, dS. \tag{23}$$

In the full PIC model, there are two ways to compute total thrust of the thruster. One way is using the above formulas and Eq. (11) or (12), which is based on the energy conversion assumption. The other way to compute the total thrust is

$$T_{total} = \dot{m} u_{exit} + p A_e, \tag{24}$$

where p is the plasma pressure and A_e is the section area of the exit. The mean value of the exit velocity u_{exit} can be obtained from the statistics of the particle velocity and number density at the exit. Using PIC method the mean exhaust velocity can be expressed as

$$u_{exit} = \left(\sum_{j=1}^{N_J} n_j u_j\right) \Big/ \sum_{j=1}^{N_J} n_j, \tag{25}$$

where N_J is the number of node at the exit.

B. Simulation model

The simulation was used to model the steady-state applied-field MPD thruster using argon propellant developed at NASA Lewis Research Center.[3] Fig. 2 shows the basic configuration which consisted of a 13 mm radius cathode and a 51 mm radius anode, both of which were 76 mm long. The model assumes that argon propellant at 0.025 g/s, 0.05 g/s, and 0.1 g/s was injected at the backplate and total discharge currents of 1000 A, 1250 A, and 1500 A. The applied magnetic field was produced by the external coils surrounding the thruster. The magnet coil with one end flush with the exit plane is 153 mm long with a 101.5 mm radius. The applied magnetic field strength was varied from 0.034 to 0.102 T by changing the coil current.

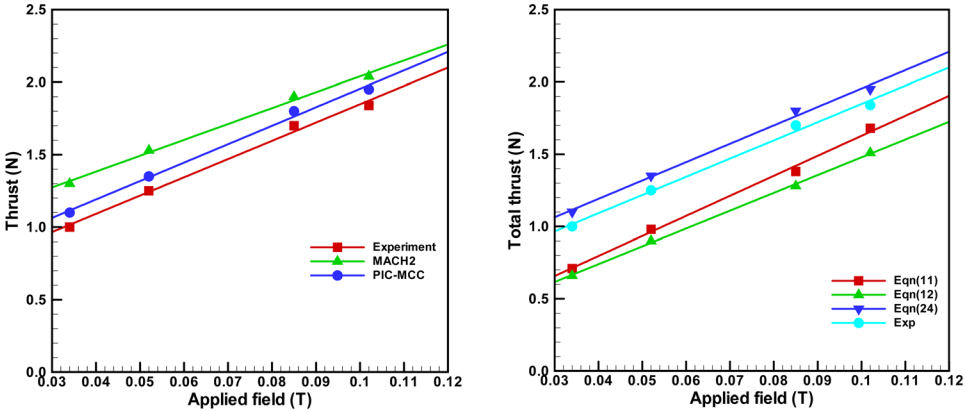

(a) Simulation with PIC-MCC method for applied field strengths of 0.034-0.102 T

(b) Total thrust with Eqn. (11), (12), (24) and experiment for applied field strengths (0.034-0.102 T)

FIG. 3. Total thrust vs applied magnetic field strength. Argon at 0.1 g/s and discharge current of 1000 A.

The discharge chamber is the primary reaction and acceleration zone; the simulation of that volume was axisymmetric 2D. The model considered the component of plasma particles to be electrons, single charged ions and neutral atoms. It was assumed that each plasma component is two dimensional in the space (z, r variation) and three dimensional coordinate ordering (z, r, θ) in velocities.

C. Boundary and initial conditions

The model defines three types of boundaries: the thruster exit is a free boundary that all particles are able to leave the simulation region through it; the backplate is a dielectric wall where particles are rebound; and the cathode and anode are conductor walls where ions and electrons are neutralization.

The anode and cathode sheaths are not included in the current model. The plasma potential boundary excluding voltage drop on anode and cathode is directly from experimental data.[3] The gas propellant modeled as neutral atoms is injected into the region as a steady background. The neutral particle temperature is set to 500 K and a Maxwellian distribution of the initial velocity is assumed in the simulation model. The initial electron temperature is 0.2 eV adding to the acceleration channel on the cathode with a shifted Maxwellian distribution in velocity.

IV. RESULTS AND DISCUSSION

A. Computation of total thrust and variation with AF-MPD thruster parameters

1. Thrust variation with applied-field

The effect of varying the applied-field strength at constant propellant mass flow and relatively constant discharge current has been studied. Thrust variations with respect to applied magnetic field strength of 0.034 T, 0.052 T, 0.085 T, and 0.102 T were calculated for steady-state with $\dot{m} = 0.1$ g/s and $I = 1000$ A. The results from PIC-MCC are presented in Fig. 3 with data from experiments and MACH2 continuum computation predictions.[3] The trend of a linearly increasing thrust with applied magnetic field strengths was captured by the simulations, consistent with the experiments, Fig. 3(a).

In order to provide a better understanding of proposed alternative methods to calculate thrust, values of total thrust using Eqs. (11), (12), and (24) are shown in Fig. 3(b).

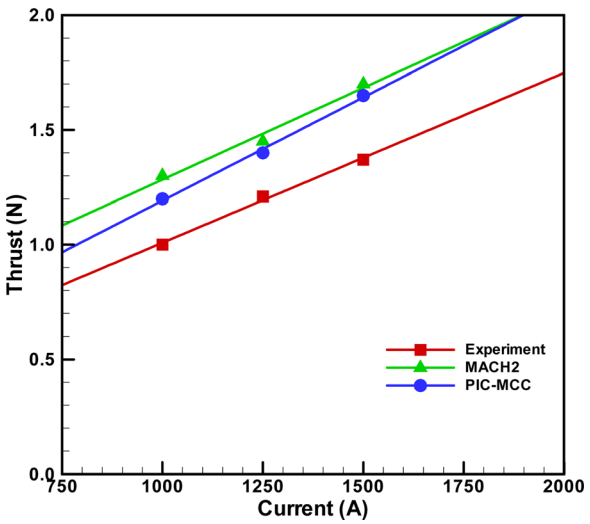

FIG. 4. Total thrust simulation with PIC-MCC method vs discharge current of 1000–1500 A. Argon at 0.1 g/s and 0.034 T.

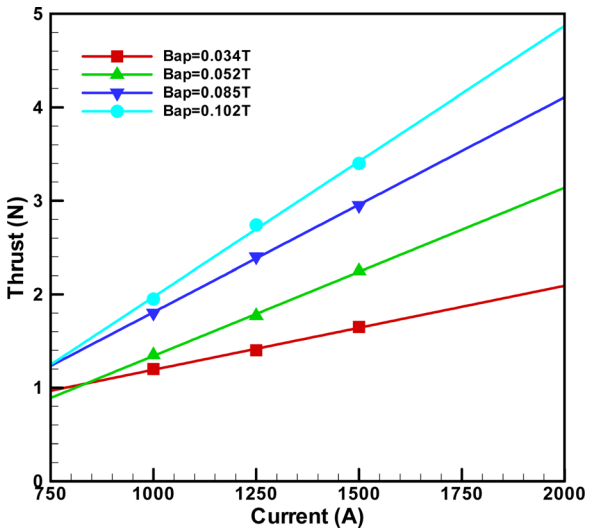

FIG. 5. Thrust vs discharge current for argon at 0.1 g/s.

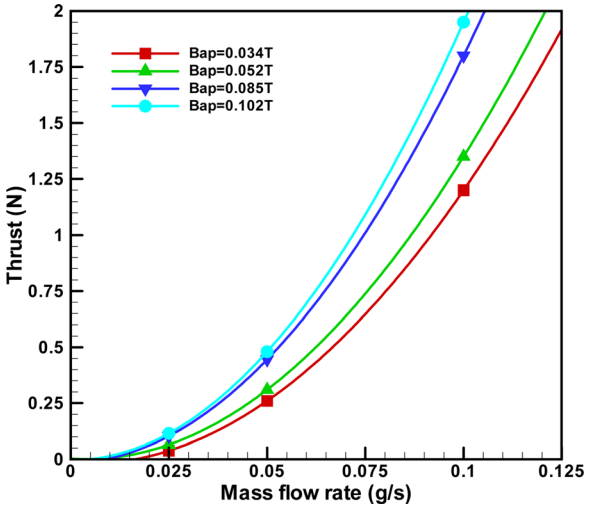

FIG. 6. Thrust vs mass flow rate for discharge current of 1000 A.

Accepting experimental data as reference, using Eq. (24) without the energy conversion assumption fits the experimental results better; the thrust values calculated by Eqs. (11) and (12) underestimated the experimental values. This result reinforces the assumption that azimuthal kinetic energy is converted completely into axially directed thrust energy is basically correct. While there is not exact agreement, however, as detailed in the accompanying paper I, the electrode voltage drops and the related energy dissipation did result in thrust loss commonly exists in the acceleration channel. These computation results and their close agreement with experimental data are taken as a basic verification of the relevance of the model and scaling of the PIC-MCC method applied here.

2. Thrust variation with discharge current

The variation of total thrust with discharge current for the case of argon propellant at 0.1 g/s and applied field of 0.034 T is shown in Fig. 4. Thrust measured in experiment along with PIC-MCC calculations are shown with values computed with the continuum code MACH2.[3] The approximate linear increase of thrust with discharge current is captured by the PIC-MCC method. The agreement obtained between PIC-MCC model and experimental values suggests that the main physical processes of the applied-field MPD thruster are included in the model. The incremental differences in magnitude are related to the component of loss attributed to the electrode losses.

Further examination of the thruster behavior is shown in Fig. 5 where thrust is presented as a function of current (1000–1500 A) and with applied magnetic field (0.034 –0.102 T) as a parameter. The approximately linear increase of thrust with discharge current is again evident for all values of increasing applied field strength which shows increasing thrust gradients for higher fields. This suggests thrust is proportional to the product of discharge current and applied field strength.

3. Thrust variation with mass flow rate

The basic mass flow rate for the computations was set at 0.1 g/s to allow comparison with experiment. Further understanding of behavior was explored by comparing results for mass flow rates of 0.1 g/s, 0.05 g/s, and 0.025 g/s in the simulation model with discharge current of 1000 A and applied fields of 0.034–0.102 T. The results shown in Fig. 6 indicate that thrust increased parabolically with increasing mass flow rate. The thrust at a given discharge current was found to increase with increasing applied field strength and mass flow rate for all cases.

B. Particle velocity and current distribution

For each time step, the plasma velocity at a specific node is defined as the average velocity of all the particles which are weighted to that node. The average axial, radial, and azimuthal velocity components for ions with argon at 0.1 g/s and 1000 A for various applied field strengths are shown in Fig. 7(a) and for electrons are shown in Fig. 7(b). The variations of these properties with discharge current are shown in Fig. 8(a) for ions and Fig. 8(b) for electrons. It can be seen that the axial velocity is dominant for the ions, and the radial velocity is dominant for the electrons. These dominant velocities increase with increasing applied magnetic field and with discharge current, respectively. The ion and electron mean velocities exceed 10 km/s and 300 km/s, respectively, owing to the presence of electromagnetic fields. The axial velocity for ions which contributes directly to thrust is dominant compared with radial and azimuthal

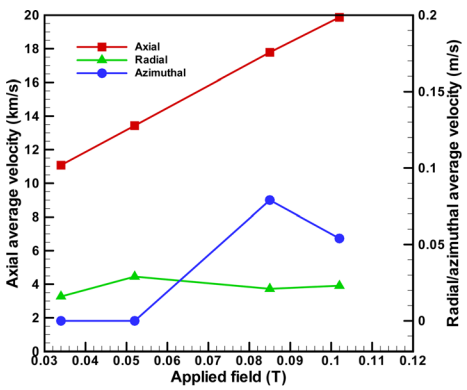

(a) Ion average velocity

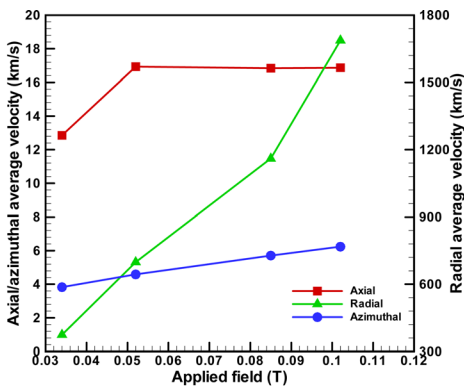

(b) Electron average velocity

FIG. 7. Plasma average velocity vs applied magnetic field strength.

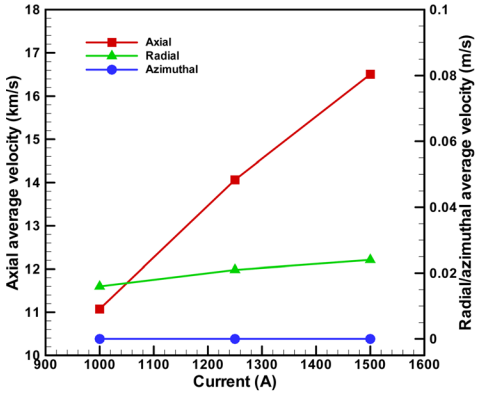

(a) Ion average velocity

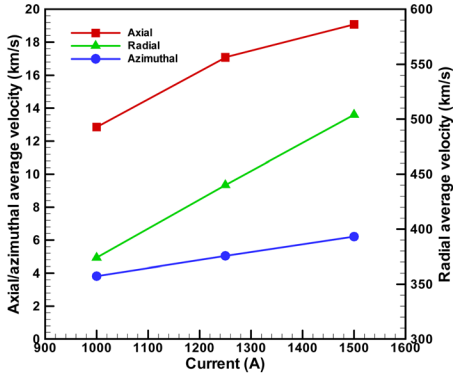

(b) Electron average velocity

FIG. 8. Plasma average velocity vs discharge current.

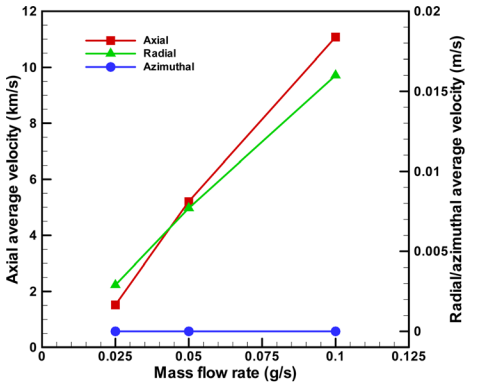

(a) Ion average velocity

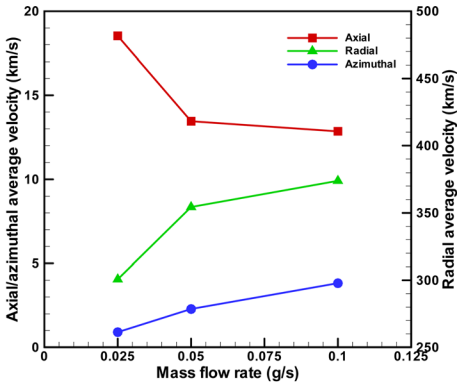

(b) Electron average velocity

FIG. 9. Plasma average velocity vs mass flow rate

components, and it increases linearly with applied field strength and discharge current. As for electrons, the radial velocity increases with increasing applied magnetic field strength and discharge current and is the major component in current conduction in the plasma. The electron axial velocity is seen to increase as discharge current rises. According to the calculation, the electron azimuthal velocity is 3–6 km/s, and it had generally linear increase of modest magnitude with increasing applied magnetic field strength and discharge current. The above noted observations of velocity behavior with respect to applied thruster conditions provide a unique insight into the particle dynamics of the AF-MPD.

At fixed discharge current and applied magnetic field, the particle velocities showed significant change with variation of mass flow rate as seen in Fig. 9. Reduction of mass flow rate from 0.1 g/s resulted in reduction of the dominant ion axial velocity and radial electron velocity. This behavior

TABLE I. Axial, radial, and azimuthal current proportions with various applied field strength and mass flow rate for total discharge current of 1000 A, 1250 A, and 1500 A.

Total current (A)	Mass flow rate (g/s)	Applied field (T)	Axial current (%)	Radial current (%)	Azimuthal current (%)
1000	0.025	0.034/0.052	0.68/0.36	99.26/99.60	0.06/0.04
		0.085/0.102	0.18/0.15	99.80/99.83	0.02/0.02
	0.05	0.034/0.052	0.67/0.36	99.27/99.60	0.06/0.04
		0.085/0.102	0.18/0.15	99.80/99.83	0.02/0.02
	0.1	0.034/0.052	0.64/0.37	99.30/99.59	0.06/0.04
		0.085/0.102	0.25/0.15	99.72/99.83	0.03/0.02
1250	0.1	0.034	0.55	99.38	0.07
		0.052	0.32	99.64	0.04
		0.085	0.18	99.80	0.02
		0.102	0.17	99.81	0.02
1500	0.1	0.034	0.48	99.44	0.08
		0.052	0.28	99.67	0.05
		0.085	0.17	99.81	0.02
		0.102	0.13	99.85	0.02

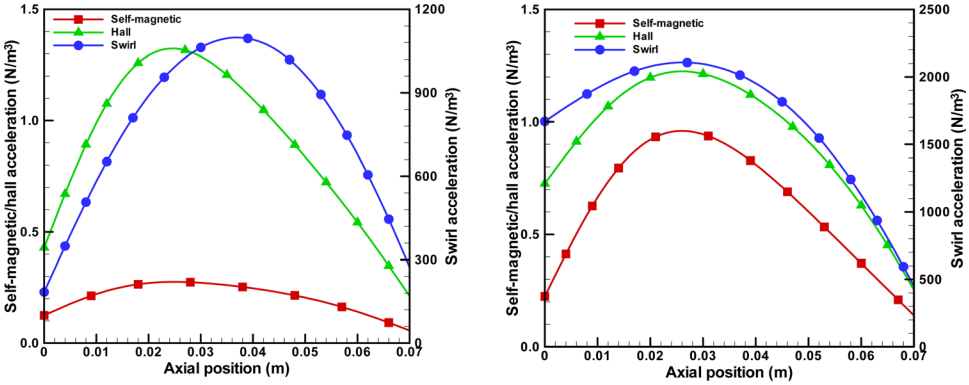

(a) Applied magnetic field B_{ap}=0.052 T (b) Applied magnetic field B_{ap}=0.102 T

FIG. 10. Axial variation of electromagnetic forces with applied field strength.

may be explained as more collisions occur between electrons and neutral particles with higher mass flow rate, and ionized particles gain energy from electrons during collisions. Further detailed studies using this type of numerical evaluation of physical behavior may prove productive.

The values of velocities defined above were the result of averaging local values of velocities throughout the interelectrode acceleration region. (Reference paper I) With the computation of particle velocities and velocity components, it is possible to directly compute local current densities, as

$$\boldsymbol{j} = e(n_i \boldsymbol{V}_i - n_e \boldsymbol{V}_e). \tag{26}$$

In order to analyze and estimate the relative magnitude of the four acceleration effects, the axial, radial, and azimuthal current proportions were calculated accounting for directional velocity components. Table I shows the relative proportions of axial, radial, and azimuthal currents for the ranges of applied field strengths (0.034–0.102 T), mass flow rates (0.025–0.1 g/s), and total discharge currents (1000 up to 1500 A). The radial component (j_r) holds the absolutely largest portion, thus the product of radial current and axial magnetic field component ($-j_r B_z$) is dominant in comparison with other Lorentz forces in the discharge chamber. This establishes that the electrons carry most of the current and are accelerated mainly by electric effect in radial direction. The azimuthal current (j_θ) is mainly produced by the plasma rotation, the proportion of which decreases with increasing applied magnetic field strength, as well as the value of axial component (j_z).

C. Acceleration mechanism contributions

The total thrust has been described in Eq. (11) as

$$T_{total} = T_{self} + T_{swirl} + T_{hall} + T_{gd}, \tag{27}$$

where the j, B components have been expressed in Eqs. (20)–(23). Based on detailed computations at axial locations throughout the acceleration channel, each of electromagnetic thrust components has been evaluated. The axial variation of electromagnetic force densities with respect to applied field strength (0.052 T in Fig. 10(a) and 0.102 T in Fig. 10(b)) for discharge current of 1000 A and mass flow rate of 0.1 g/s at the axial cross section $r = 32$ mm is presented in Fig. 10. Self-magnetic and Hall forces are smaller than the swirl component. An increase of applied field strength increases the swirl component significantly. Each of the components shows behavior with lower values at entry and exit with a maximum value toward mid-axial position.

The variation of thrust components with a variation of axial position with discharge current as a parameter is shown in Fig. 11(a). All components increase in magnitude with increasing current, and there is a tendency for the point of maximum value to shift forward toward the entry. A simulation of the axial variation of the components with mass flow rate as a parameter is shown in Fig. 11(b). In general, magnitudes drop with reduced mass flow rate, and the axial variation functional form is maintained.

The thrust components resulting from the four acceleration modes are shown in Table II. The results show that swirl acceleration is the main thrust production for all cases in

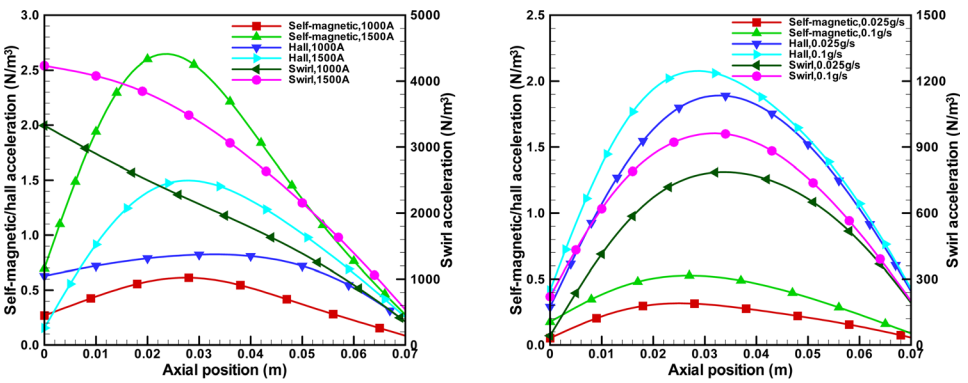

(a) Electromagnetic acceleration with various current (b) Electromagnetic acceleration with various mass flow rate

FIG. 11. Axial variation of electromagnetic forces with discharge current and mass flow rate.

TABLE II. Average self-magnetic, Hall, swirl, and gas-dynamic acceleration contributor with various applied field strengths and mass flow rate for total discharge current of 1000 A, 1250 A, and 1500 A.

Total current (A)	Mass flow rate (g/s)	Applied field strength (T)	Self-magnetic thrust (N)	Hall thrust (N)	Swirl thrust (N)	Gas-dynamic thrust (N)
1000	0.025	0.034/0.052	0.0003/0.0004	0.0027/0.0059	0.016/0.031	0.0038/0.0068
		0.085/0.102	0.0005/0.0008	0.0091/0.0188	0.052/0.062	0.0125/0.0176
	0.05	0.034/0.052	0.0001/0.0005	0.0020/0.0041	0.244/0.246	0.0030/0.0321
		0.085/0.102	0.0002/0.0005	0.0172/0.0212	0.314/0.355	0.0437/0.0719
	0.1	0.034/0.052	0.0012/0.0010	0.0381/0.0382	0.642/0.879	0.0289/0.0612
		0.085/0.102	0.0009/0.0009	0.0375/0.0377	1.342/1.486	0.0805/0.1512
1250	0.1	0.034	0.0027	0.0576	0.892	0.0546
		0.052	0.0022	0.0536	1.186	0.1124
		0.085	0.0018	0.0518	1.895	0.1373
		0.102	0.0015	0.0541	2.169	0.1823
1500	0.1	0.034	0.0039	0.0728	1.325	0.0786
		0.052	0.0037	0.0758	1.594	0.2022
		0.085	0.0029	0.0633	2.231	0.2379
		0.102	0.0020	0.0710	2.569	0.3763

applied field MPD thruster when the rotation energy is converted into axial thrust energy through a magnetic nozzle. The self-magnetic acceleration is small compared to the other acceleration effects. The Hall acceleration force produced by the azimuthal current and applied magnetic field is insensitive to the change of externally applied field; the effects of magnetic field on electron swirl are small, the value of which slightly increases when the current is raised. The acceleration contributions of Hall reaction force and gas-dynamic force lie between self-magnetic and swirl modes. The gas-dynamic acceleration force increases with increasing applied magnetic field strength, discharge current, and mass flow rate. In summary, the self-magnetic, Hall, gas-dynamic, and swirl acceleration mechanisms were found to be in the approximate ratios of 1:10:10:100 in this investigation.

The force terms tending to put the plasma into rotation are $j_r B_z$ and $j_z B_r$. The value of j_r dominates the total current. Accordingly (Eq. (21)), the swirl force predominates in the electromagnetic forces. The conversion of the rotational energy produced by swirl acceleration to directed axial energy results in the dominant thrust. The simulations with PIC-MCC method suggest that the currents are mainly carried by electrons, and that thrust production is done mostly by the ions, which gain the energy by the collisions with electrons and acceleration effect of the electromagnetic force associated with the applied field.

V. CONCLUSION

The PIC-MCC method was used to model the acceleration mechanisms in applied-field MPD thrusters. The simulation model of a 100 kW applied-field MPD thruster considered that each plasma component was two dimensional in space (r, z) and three dimensional (r, θ, z) in velocities. Under the condition of the mass flow rate from 0.025 g/s to 0.1 g/s of argon propellant and discharge current of 1000–1500 A, the applied magnetic field strength was varied from 0.034 T to 0.102 T.

The new approach was applied to calculate total thrust values that were then compared with experimental data and also the results of modeling with an MHD numerical solution with the MACH2 solver. The trend of approximately linearly increasing thrust with applied magnetic field strengths was approximately captured by the simulations, which were consistent with the experiments and verified with the theoretical model. Investigations of the acceleration model based on the underlying theory indicated the swirl acceleration mechanism was the dominant contributor to plasma acceleration, and self-magnetic, Hall, gas-dynamic, and swirl acceleration mechanisms were in an approximate ratio of 1:10:10:100. The Hall acceleration produced mainly by electron swirl was insensitive to the change of externally applied magnetic field strength and slightly increased with increasing the current. The self-magnetic acceleration could be normally negligible for all cases, while gas-dynamic acceleration contributor increased with increasing applied magnetic field strength, discharge current, and mass flow rate.

ACKNOWLEDGMENTS

The authors wish to thank Associate Professor Joseph Wang of the University of Southern California (USC) for his valuable advice and assistance to the PIC-MCC method of this paper.

[1]E. Y. Choueiri, J. Propul. Power **14**(5), 744 (1998).
[2]H. G. James, AIAA 2003-4841 (2003).
[3]P. G. Mikellides, P. J. Turchi, and N. F. Roderick, J. Propul. Power **16**(5), 887 (2000).
[4]D. B. Fradkin, Ph.D. dissertation, Princeton University, Princeton, 1973.
[5]D. B. Fradkin, A. W. Blackstock, D. J. Roehling, T. F. Stratton, M. Williams, and K. W. Liewer, AIAA J. **8**(5), 886 (1970).
[6]R. M. Mayers, J. Propul. Power **11**(2), 343 (1990).
[7]R. M. Mayers, J. Propul. Power **9**(5), 781 (1993).
[8]G. Krulle, AIAA 1972-501 (1972).
[9]M. Tanaka and I. Kimura, J. Propul. Power **4**(5), 428 (1988).
[10]A. Sasoh and Y. Arakawa, IEPC 1991-062 (1991).
[11]Y. Arakawa and A. Sasoh, J. Propul. Power **5**(3), 301 (1989).
[12]P. G. Mikellides and P. J. Turchi, J. Propul. Power **16**(5), 894 (2000).

[13]A. Fruchtman, K. Takahashi, C. Charles, and R. W. Boswell, Phys. Plasmas **19**(3), 3507 (2012).
[14]H. Tahara, Y. Kagaya, and T. Yoshikawa, J. Propul. Power **13**(5), 651 (1997).
[15]H. G. James, AIAA 2004-3470 (2004).
[16]G. J. Robert, *Physics of Electric Propulsion* (McGraw-Hill, New York, 1968), pp. 240–245.
[17]A. Fruchtman, Phys. Plasmas **10**(5), 2100 (2003).
[18]V. B. Tikhonov, S. A. Semenikhin, V. A. Alexandrov, G. A. Dyakonov, and G. A. Popov, IEPC 1993-076 (1993).
[19]G. Krulle, M. Auweter-Kurtz, and A. Sasoh, J. Propul. Power **14**(5), 754 (1998).
[20]A. Sasoh, Phys. Plasmas **1**(3), 464 (1994).
[21]A. D. Kodys and E. Y. Choueiri, AIAA 2005-4247 (2005).
[22]Y. Arakawa and A. Sasoh, J. Propul. Power **8**(1), 98 (1992).